Investigating an indirect aviation effect on mid-latitude cirrus clouds - linking lidar derived optical properties to in-situ measurements

Silke Groß[1], Tina Jurkat-Witschas[1], Qiang Li[1], Martin Wirth[1], Benedikt Urbanek[1], Martina Krämer[2,3], Ralf Weigel[3], Christiane Voigt[1,3]

[1]Deutsches Zentrum für Luft- und Raumfahrt (DLR), Institut für Physik der Atmosphäre, Wessling, 82234, Germany
[2]Forschungszentrum Jülich, Institute of Energy and Climate Research, Jülich, Germany
[3]Johannes Gutenberg-University, Institut für Physik der Atmosphäre, Mainz, Germany

Correspondence to: Silke Groß (silke.gross@dlr.de)

Abstract.

Aviation has a large impact on the Earth's atmosphere and climate by various processes. Line shaped contrails and contrail cirrus clouds lead to changes in the natural cirrus cloud cover, and have a major contribution to the effective radiative forcing from aviation. In addition, aviation induced aerosols might also change the microphysical properties and optical properties of naturally formed cirrus clouds. Latter aerosol-cloud interactions show large differences in the resulting effective radiative forcing and our understanding on how aviation induced aerosols affect cirrus cloud properties is still poor. Up to now, observations of this aviation induced aerosol effect are rare. In this study, we use combined airborne lidar and in-situ ice cloud measurements to investigate differences in the microphysical and optical properties of naturally formed cirrus clouds, which formed in regions that are highly affected by aviation induced aerosol emissions and of those, which formed in regions rather unaffected by aviation. Urbanek et al., 2018 showed that those cirrus clouds, which are more affected by aviation induced soot emission, are characterized by larger values of the particle linear depolarization ratio (PLRD). In this follow-on study we relate collocated lidar measurements performed aboard HALO during the ML-CIRRUS mission of the particle linear depolarization ratio with in-situ cloud probe measurements of the number concentration and effective diameter of the ice particles. We find, that clouds with higher PLRD also show larger mean effective ice particle diameters connected to decreased ice particle number concentration, than the cirrus clouds, which evolved in more pristine regions with only little impact from aviation.

1. Introduction

Aviation has a large impact on the Earth's radiation budget and atmosphere (Lee et al., 2021) by various interactions; e.g. aerosols and trace gases are emitted, which directly interact with incoming and outgoing radiation (Lund et al., 2017). Line shaped contrails can form in the exhaust plume of an aircraft (Voigt et al., 2010; Burkhardt et al., 2010) and might evolve into contrail induced cirrus clouds in the aftermath (e.g. Haywood et al., 2009). A lot of research activities have been performed over the last years to measure (Heymsfield et al., 2010a; Voigt et al., 2011; Voigt et al., 2017) and understand contrails and

contrail cirrus (e.g. Kärcher et al., 2015; Schuman et al., 2017), and to investigate their climate effect (Burkhardt and Kärcher, 2011; Kärcher, 2018; Bock and Burkhardt, 2019; Quaas et al., 2021). Contrails and contrail induced cirrus clouds are supposed to have the largest aviation induced impact on the Earth's radiation budget with a clearly warming effect (Lee et al., 2021). Recent studies show, that the climate impact from contrails can be reduced by burning sustainable aviation fuels with a low aromatic content (Moore et al., Nature, 2017; Burkhardt et al., 2018; Voigt et al., 2021; Bräuer et al., 2021) or by climate friendly flight routing (Grewe et al., 2018). Contrails can further lead to an increase in the cirrus cloud optical properties (Tesche et al., 2016), and to changes in their ice crystal effective diameter (Heywood et al., 2009) and ice crystal number concentration (Majani et al., 2022).

Besides contrail formation and its effect on already existing clouds, aviation induced aerosols might also act as ice nuclei (INP) for naturally formed clouds. The aerosols change the microphysical properties; i.e. number concentration and size of ice crystals of naturally formed cirrus clouds (Kärcher, 2017) and thus their optical and radiative effect. Model studies investigating the impact of this aviation induced aerosol-cloud interaction show large differences in the resulting effective radiative forcing. Particularly the estimates of the impact of emitted soot particles on cirrus clouds are connected with large uncertainties. Several studies focused on the impact of aviation soot on cirrus clouds and thus on the resulting climate effect (e.g. Hendricks et al., 2005, 2011; Liu et al., 2009; Gettelman and Chen, 2013). Large differences in the magnitude and even in the sign of the effect (Penner et al., 2009, 2018; Zhou and Penner, 2014) were reported. The uncertainties in the estimate of the climate effect of aviation soot are mainly driven by the assumed efficiencies of soot particles to act as IN (Righi et al., 2021). While some laboratory studies found soot particles to be efficient IN (Möhler et al., 2005; Hoose and Möhler, 2012), others indicate soot particles are not efficient IN (DeMott et al., 1999). In a recent laboratory study, Mahrt et al., (2020) found that soot particles would increase their efficiency to act as IN after being pre-processed within contrails. This indicates an overestimation of the soot effect in some of the model studies.

Although the understanding of the aviation's impact on the climate system has improved over the last years, many uncertainties remain. But, observations of an aviation induced indirect aerosol effect on cirrus clouds are rare. Urbanek et al. (2018) analyzed airborne lidar measurements over Europe, performed during the ML-CIRRUS mission (Voigt et al., 2017), and found larger median values of the particle linear depolarization ratio (PLDR) of cirrus clouds formed in air traffic regions compared to those evolved in regions with only little impact from aviation. Their analysis further showed lower supersaturation for those clouds with high PLDR formed in air traffic regions, which they interpreted as a signature of more heterogeneous freezing. The measurement study by Urbanek et al. (1998) is one of the first that could show traces of an indirect aerosol effect from aviation. During the first COVID-19 curfew in spring 2020, civil aviation over Europe was reduced by up to almost 90% (www.eurocontro.int/cov19). This reduction caused a unique opportunity to study the effect of aviation on cirrus clouds. Li and Groß (2021) used spaceborne lidar measurements onboard the CALIPSO satellite (Winker et al., 2010) in March and April 2020 to investigate differences in cloud occurrence and optical properties compared to former years in the same time period. They found less cirrus occurence mainly for colder height levels and for thinner cirrus clouds. Those findings were interpreted as a reduction of contrails and contrail induced cloudiness due to reduced aviation. Schumann et al. (2021a, b) investigated the

65 changes in contrail occurrence and the formation of persistent contrails by performing contrail simulations with the contrail cirrus prediction model CoCiP (Schumann et al., 2012). They found that changes in the cirrus cloud occurrence from March to August 2020, compared to the same period in 2019, was partly caused by the air traffic reduction. Theo et al., 2022 found a significant decrease in contrail cirrus cover and energy forcing in 2020, when comparing to modelled contrail cirrus effects in the northern Atlantic flight corridor regions from 2016 to 2019.

70 Furthermore, a significant decrease in the mean PLDR of cirrus clouds was found in spring 2020 compared to former years (Li and Groß, 2021), which can be interpreted as a reduced, aviation induced and indirect effect on naturally formed cirrus clouds. An integrated study, using aircraft, satellite and modelling data, showed a reduction of the aerosol optical depth over Europe in May 2020 (Voigt et al., 2022), which was partly caused by the 80% decline of air traffic. It furthermore led to a reduction in contrail cover and as a consequence in radiative forcing. Voigt et al. (2022) also showed reduced effective optical

75 depth of the cirrus clouds compared to former years connected with reduced PLDR. Looking at long-term cirrus observations using CALIPSO measurements, Li and Groß (2022) found a significant increase in the PLDR over the last years, which is clearly correlated to the increase in the number of flights over Europe. However, besides these advances in observing the change in optical properties due to the impact of aviation induced soot, the link to the microphysical properties of the cirrus clouds is still missing. In a recent study, Zhu et al., (2022) examined CALIPSO satellite observations during the COVID-19

80 lockdowns and found a significant increase in ice crystal number concentration (N_{part}), which they linked to an increase in homogeneous freezing due reduced aviation.

In this study we extend the work by Urbanek et al. (2018) using combined lidar and in-situ measurements aboard HALO performed during the ML-CIRRUS mission (Voigt et al., 2017), to investigate differences in the microphysical properties of natural cirrus clouds formed in air traffic regions and those formed in regions less effected from aviation. For this, we use the

85 same clouds that were investigated within our former study (Urbanek et al., 2018). In section 2, we will present the campaign and the measurements. In section 3, we will show the results focusing first on two case studies of different cirrus cloud types and afterwards on all the cloud measurements with collocated lidar and in-situ measurements. Section 4 will discuss the results and conclude this study.

2. Method

90 ### 2.1. ML-CIRRUS Campaign

The ML-CIRRUS campaign was conducted in March/April 2014 to study cirrus clouds in meteorological regimes typical for mid-latitudes. ML-CIRRUS aimed to investigate contrail cirrus, as well as to observe differences between anthropogenic and natural cirrus clouds. To achieve this goal, measurement flights with the German High Altitude and Long Range research aircraft (HALO), equipped with a combined remote sensing (including airborne lidar) and in-situ (including cloud probes)

95 payload, were performed out of Oberpfaffenhofen. An overview of the mission, the performed research flights and their main focus can be found in Voigt et al. (2017). Overall, 16 flights were performed covering the whole range of the mid-latitudes;

from 36 to 58°N and from the Atlantic Ocean (~15°W) to Central Europe (~15°E). However, only eight of the 16 flights were designed in a way, that they provide coordinated lidar and in-situ measurements. The sampling strategy during these flights were as follows: First, the HALO aircraft flew at higher altitudes above the cloud for sounding the cirrus clouds with the lidar (lidar leg). Subsequently, the same cirrus clouds were probed by in-situ measurements at several flight altitudes within the cirrus clouds (in-situ leg). Typical lidar legs took about 30 min to 50 min; with a typical aircraft speed of 200 m/s that result in an observed cloud dimension of about 360 km to 600 km. The in-situ legs took a minimum of 10 min per constant flight altitude. For our study only these eight flights with coordinated lidar and in-situ measurements are relevant. Urbanek et al. (2018) grouped these flights respectively if the cirrus clouds developed in regions with enhanced background aerosols from aviation or in regions rather unaffected from aviation. By means of 24-hr backward trajectories calculated with the trajectory module of CLaMS (McKenna et al., 2002), they investigated the maximum cloud ice water content to determine the most probable location of the cirrus development and compared that to maps of enhanced background aerosols due to aircraft emissions (Stettler et al., 2013). Information on the flights (including their Mission ID to make it comparable to Urbanek et al. (2018)) are given in Table 1.

Table 1: Overview of the combined in-situ and lidar research missions during ML-CIRRUS showing the Mission ID, Date, Measurement region and scope of the mission, median PLDR, temperatures of in-situ measurements and altitude range. Listed are only those missions with combined lidar and in-situ measurements. Entries in dark blue show flight segments with cirrus clouds that have been affected by aviation induced aerosols (according to Urbanek et al., 2018), those in light blue indicate flight segments with cirrus clouds developed in regions with no or less aviation. The flight missions indicated in bold letters are shown in detail in the case studies.

ID	Date	Region	Scope	Median PLDR	Temperature / K	Altitude / km
M4	**26 Mar.**	**North Atlantic flight corridor**	**Contrails, contrail cirrus**	**0.51**	**208 - 214, 216**	**10 – 12**
M5	27 Mar.	Germany, Italy	WCB cirrus	0.40	214, 215, 216, 220	8 – 10
M6	29 Mar.	France, Spain	Lee wave cirrus, WCB, jet stream	0.41	210, 211, 213, 214, 215	7 – 11
M7	1 Apr.	Germany	Cirrus, contrail cirrus	0.46	210 - 217	10 – 11
M8	3 Apr.	Germany	WCB cirrus	0.38	212 - 217	9.5 – 10.5
M9	4 Apr.	Spain	Jet stream	0.34	213 - 216	8 – 12
M11	7 Apr.	Germany	Contrail cirrus	0.39	208 - 214, 216, 217	9 – 11
M14	**11 Apr.**	**Great Britain**	**WCB cirrus**	**0.48**	**226, 227**	**8 - 12**

2.2. WALES lidar system

The WALES (WAter vapor Lidar Experiment in Space; Wirth et al., 2009) lidar is a combined high spectral resolution lidar (HSRL) and differential absorption lidar (DIAL) system, which was developed and built at the Institute of Atmospheric Physics of the German Aerospace Center. It measures directly the extinction coefficient at 532 nm, using the HSRL technique with a high vertical resolution of 15 m and of typically 0.2s resolution in time (Esselborn et al., 2008). Additionally, the system is equipped with polarization sensitive channels at 532 and 1064 nm. For determining the particle linear polarization ratio (PLDR), which is the ratio of the measured perpendicular and the parallel component of polarization of the backscattered light, we apply the ±45° calibration method (Freudenthaler et al., 2009), and thus achieve an absolute accuracy of 5 percentage points at typical cirrus PLDR values of about 0.35 to 0.55.

To assure that high altitude aerosol residuals and liquid or mixed phase clouds are excluded from our study, we restrict the considered data to measurements of temperature ranges below 235 K and of a backscatter ratio (R) above a threshold of R=3. The backscatter ratio is defined as the ratio of the total backscatter coefficient (molecules and aerosol/cloud particles) to the molecular backscatter coefficient. This threshold was determined by carefully investigating all flights with lofted aerosol layers (Urbanek et al., 2018). Sensitivity studies showed, that the further analysis only weakly depend on the chosen R value within a range from R=2 to R=25.

2.3. In-situ Instrumentation

Particle number concentrations (N_{par}) and effective diameter (D_{eff}) are calculated using a composite of particle size distributions from three cloud probes, applying scattering detectors and light attenuation on optical arrays. Small particles in the size range from 3 to 50 µm were detected by the CAS-DLR (Voigt et al. 2017, Kleine et al. 2018). The data have been grouped into 16 size bins, assuming rotationally symmetrical ellipsoids of random orientation with aspect ratios of 0.75, to avoid Mie-ambiguities in the scattering signals. Larger particles were detected by a CIP (Cloud Imaging Probe; CIP-UniM) as part of the CCP (Cloud combination probe) and a PIP (Precipitation Imaging Probe) instrument (Weigel et al., 2016). Maximum dimension diameters were derived from 2D images and number concentrations were corrected for compression effects according to Weigel et al. 2016. The CIP was operated in the size range from 15 and 960 µm, the PIP has been operated in the size range from 100 to 6400 µm. The effective diameter is calculated from the effective radius (2*reff) according to Schumann et al. 2011. The data have been averaged over 5 s intervals. For the majority of flights the combined particle size distribution of the CAS, the CIP and the PIP was used, which is the same data set as used in the work of Righi et al., 2020 and Wang et al., 2023.

For the flight of 7 March 2014, only data from the NIXE-CAPS (Novel Ice Experiment–Cloud Aerosol and Precipitation Spectrometer; Krämer et al., 2016; Costa et al., 2017) instrument are available due to a failure of the CIP instrument. NIXE-CAPS is a combination probe that integrates two techniques for measuring the particle size distribution (PSD): the PSD of particles 0.6 to 50 µm in diameter is measured with NIXE's Cloud and Aerosol Spectrometer (NIXE-CAS) using light scattered

from individual particles that pass through a focused laser beam. For measurements of particles 15–937 μm in diameter,
NIXE's Cloud Imaging Probe (NIXE-CIP-grey threshold), which utilizes the optical array probe (OAP) technique, is used. Using the data analysis routines collected in the NIXE-Lib, the PSDs of both instruments are analyzed simultaneously, whereby various error analyzes and corrections are applied, including a correction of possible shattering of large ice crystals at the inlet tips. The data of NIXE-CAPS and the combined cloud probes are redundant which was helpful in case of a failure but also to assure good quality and consistency in the obtained data set. Comparison of the data sets for days when the two combined PSD were available showed in general a good agreement. As we only discuss relative changes in Npar and Deff, small differences arising by the use of different probes should not affect the results.

In addition, measurements of the meteorological state parameters (e.g. T, RHi) at flight altitude were performed with Basic HALO Measurement and Sensor System (BAHAMAS; Giez et al., 2023).

3. Results

In a previous study (Urbanek et al., 2018) we found, that cirrus clouds evolved in regions with enhanced air traffic show larger mean values of the PLDR than cirrus clouds forming in regions rather unaffected from aviation. In this study we extend the investigation of an impact of aviation on the microphysical properties of the cirrus clouds by comparing in-situ measurements performed within these two cloud classes (of high and low PLDR). During the ML-CIRRUS campaign, eight missions were performed which provide coordinated lidar and in-situ measurements (Table 1). The results of those coordinated measurements will be presented in the following. Two case studies show the differences of optical and microphysical properties of similar cirrus cloud types; one formed in a region of enhanced background aerosols due to aircraft emission and one evolved in rather from aviation unaffected airmasses. One of the two case studies show measurements of cirrus clouds strongly affected by embedded contrails and the other of a warm conveyor belt cirrus. Those cases represent two of the main cirrus types in the European Mid-Latitudes. In a next step, we investigate the overall distribution of optical and microphysical properties of the observed cirrus clouds.

3.1. Case study – Contrail Cirrus

The first case study we choose for the comparison is a cirrus case with embedded fresh contrails (Wang et al., 2022). For the clouds observed on 26 March 2014 and 7 April 2014, the contrail cirrus prediction model (CoCiP; Schumann 2012) indicated a large amount of embedded fresh contrails within the cirrus cloud (Urbanek, 2019). Back-trajectory analysis (Urbanek et al., 2018) indicate the origin of the cloud on 26 March over the North Atlantic with enhanced background aerosol due to aviation emission. The cirrus cloud on 7 April evolved further south over the Atlantic Ocean, in an area that is much less affected by aviation exhaust (Stettler et al., 2013).

The time-height cross-sections of the PLDR of the two cirrus clouds with embedded fresh contrails is shown in Figure 1 ((a)

180   and (b)) along with the density distributions ((c) and (d)) of the particle linear depolarization ratio (PLDR). Both cirrus clouds

are in approximately the same temperature and height range, so they are well comparable. The values of the PLDR of the two

cirrus clouds is quite different. The cirrus on 26 March 2014 shows larger values of the PLDR than the cirrus cloud on 7 April

2014. For the first one, we find values up to 0.6, while the PLDR of the cloud on the 7 April barely exceeds 0.45. The mode

of the PLDR distribution within the cirrus cloud on 26 April is 0.54, its median 0.52. In contrast, the mode and median of the

185   PLDR distribution of the cirrus cloud on 7 April 2014 is much lower at values of 0.34 and 0.29, respectively. Both cirrus

clouds show a large number of embedded contrails and are still different with respect to their PLDR. Thus, the freshly

embedded contrails cannot be interpreted as a cause for the significant differences in the PLDR.

190
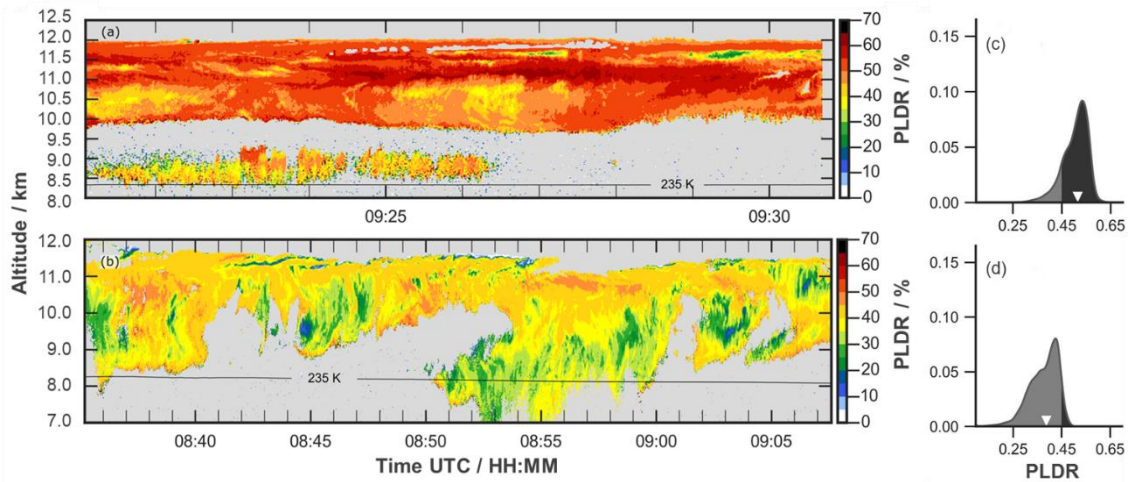
Figure 1: Time-height cross-section of the particle linear depolarization ratio (PLDR) for the contrail affected cirrus cloud cases on 26 March (a) and 07 April 2014 (b), and the frequency distribution of the measured PLDR (c, d) of the cloud parts at temperature regions below 235 K. The color coding of the PLDR distribution (c and d) marks the threshold defined by Urbanek et al., 2018 for high (dark grey) and low (light grey) PLDR values.

195

In-situ measurements were performed within the cirrus cloud at an altitude of approximately 11 km and show mean relative

humidity with respect to ice (RHi) and temperature values of about 100% and about 208 to 217 K, respectively, for both clouds.

So, any differences due to different measurement conditions within the cloud are not expected. For 26 March 2014, combined

CAS-DLR/CIP-UniM are used. For 7 March 2014 CIP-UniM data are missing, due to an error in the data acquisition. Thus,

200   we performed the same data analysis using the NIXE CAPs data instead. As CAS-DLR/CIP-UniM and NIXE-CAPS data show

agreement on all other days, this has no effect on the result. The distributions of the derived D_{eff} are narrow for both cirrus

cases, with the main values below 100 µm (Figure 2) potentially due to the high number of embedded contrails. The median

D_{eff} value for the cirrus cloud measured on 26 March of 58.5 µm is slightly larger than the median value of 53.2 µm measured on 7 April 2014. Differences are also found for the measured N_{par} for the two cloud cases. The distribution for the cirrus cloud

205   evolving in regions with large amount of aviation exhaust (26 March) shows a median value of 0.04 cm^{-3}. In contrast, the distribution of N_{par} on 7 April is broader and shows a larger median value of 0.15 cm^{-3}. In summary, the case study shows larger median effective diameter and lower number concentration for the aviation impacted cloud with the high particle linear depolarization ratio mode. This result will be discussed more in the conclusion.
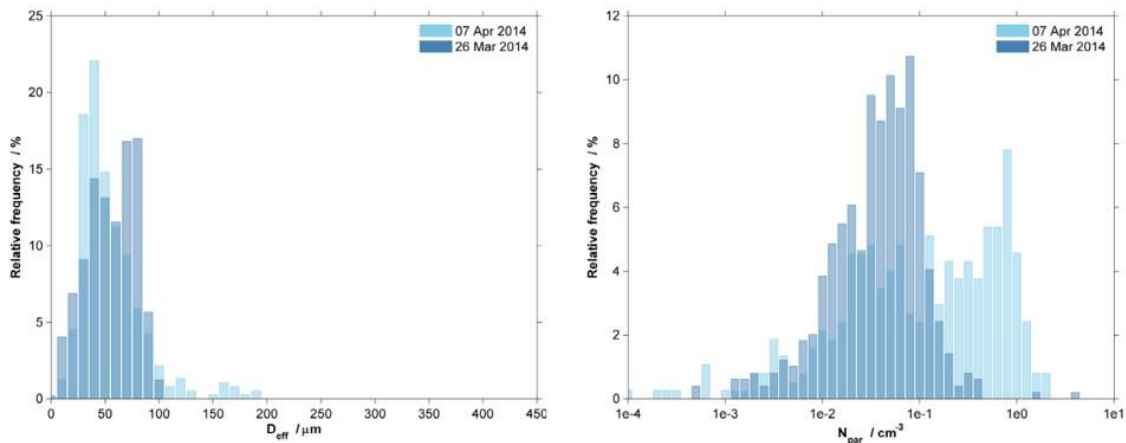
210

Figure 2: Relative distribution of the retrieved effective diameter D_{eff} (left) and ice particle number concentration N_{par} (right) for the contrail affected cirrus cloud cases on 26 March (dark blue) and 7 April (light blue) 2014 from in-situ measurements during ML-CIRRUS.

3.2. Case study – Warm Conveyor Belt Cirrus

215   In a second case study, we compare the optical and microphysical properties of warm conveyor belt (WCB) cirrus. WCBs are a typical flow structure of the mid-latitudes leading to increased precipitation (Eckhardt et al., 2004). A warm conveyor belt (WCB) is characterized by warm humid air that is lifted fast (~ 10 cm/s; Browning, 1971) from the boundary layer to the upper troposphere on the time scale of 2 days. During the lifting process, liquid clouds form and freeze. This leads eventually to pure ice clouds. During ML-CIRRUS, we were able to observe and probe four cases of WCB cirrus (see Table 1). For this study,

220   we choose the cloud observed on 27 March 2014 and on 11 April 2014. To ensure that we are comparing clouds in approximately the same stage of lifetime, we use the cirrus lifetime classification method presented by Urbanek et al. (2017). The classification scheme is based on previous studies using differences of the RHi distribution in clouds at different stages of evolution (Groß et al., 2014). Based on combined temperature information and water vapor lidar measurements, it identifies regions outside and inside the cloud of supersaturation with respect to ice, heterogeneous and homogeneous nucleation,

225   depositional growth and ice sublimation in the 2-D field along the flight track. Only about 0.4-0.5% of the clouds are in the nucleation mode, and about 30% are in the deposition mode. The majority of both clouds (~70%), however, is in the

sublimation mode. This analysis proves that both clouds are well comparable and that effects that might be caused by different evolution stages of the cirrus clouds can be excluded. Trajectory analysis for the two clouds shows, that the first one evolved in rather clean, from aviation exhaust unaffected situations over northern Africa / the Mediterranean, while the nucleation
230 process for the second one took place over the north Atlantic region, highly affected by air-traffic exhaust (Urbanek et al., 2018).

Figure 3 shows the time-height cross-sections ((a) and (b)) and density distributions ((c) and (d)) of the particle linear depolarization ratio (PLDR). While the PLDR of the WCB cirrus on 27 March 2014 does not exceed values of 0.55, the
235 PLDR of the WCB cirrus on 11 April 2014 shows values as high as 0.7 at the top and in the lower part of the cloud. Considering all the measurement points within the observed WCB cirrus on 27 March, the overall distribution of PLDR has its maximum at a value of 0.41; the median of the distribution is at 0.4. In contrast, the distribution of the PLDR of the WCB cirrus on 11 April has its maximum at 0.5 and its median at a value of 0.48. As we find the differences in the measured PLDR for both WCB cases, and as their stage of evolution is approximately the same, we suggest that neither the cirrus
240 cloud type nor its lifetime has an effect on the differences in the PLDR.
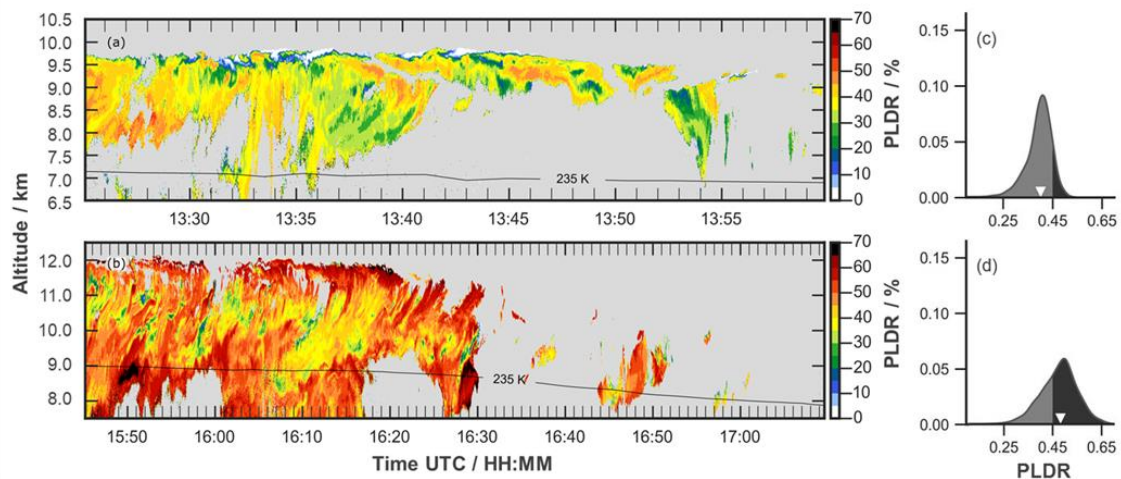
Figure 3: Time-height cross-section of particle linear depolarization ratio (PLDR) for the WCB cirrus observed on 27 March (a) and 11 April 2014 (b), and the frequency distribution of the measured PLDR (c, d) of the cloud parts at height regions below 235 K.
245 **The color coding of the PLDR distribution marks the threshold defined by Urbanek et al., 2018 for clouds characterized by high (dark grey) and low (light grey) PLDR values.**

The in-situ flight track for both clouds were performed approximately in the middle of the clouds' vertical extension; at about 9 km altitude for the cloud on the 27 March and at about 9.5 km altitude for the cloud on the 11 April. The relative humidity with respect to ice (RHi) along both flight tracks (Kaufmann et al., 2019) agrees well for both clouds with mean values of
250 105% and 104%. However, although the flights took place in approximately the same height range, the temperatures are quite

different with a mean value of 216 K for the measurements on 27 March and a mean value of 225 K for the flight track of 11 April. Thus the comparison of the cloud microphysical properties have to be treated with care. The distribution of D_{eff} (Figure 4; left) for the WCB cirrus on 27 March 2014 has a narrow mono-modal structure with its maximum between about 80 to 110 µm. In contrast, D_{eff} within the WCB cirrus on 11 April shows a broader distribution with its maximum at about 200 µm and

255   a second smaller mode at about 100-120 µm. The overall mean (median) values of D_{eff} for the WCB cirrus on 27 March and 11 April are 93.25 µm (95.12 µm) and 198.21 µm (193.78 µm), respectively. The distributions of N_{par} show only little differences for the two WCB cirrus cases. Both distributions show a skewness towards smaller values and a median at about 0.02 cm^{-3} at 27 March and of 0.04 cm^{-3} for 11 April. However, the temperatures in which the in-situ data were sampled are quite different and thus might have a quite significant impact on the retrieved results, which will be discussed in Section 3.3.

260   Earlier the day on 11 April (~ 7:50-8:25 UTC) we performed in-situ measurements within the same cloud system at a height of about 10.5 km and a temperature range of 218-219 K. The mean (median) values of Deff and Npar are 132,09 µm (131,87 µm) and 0.07 cm^{-3} (0,02 cm^{-3}). Unfortunately, now lidar measurements are available at the same time to make the full use of this time range.
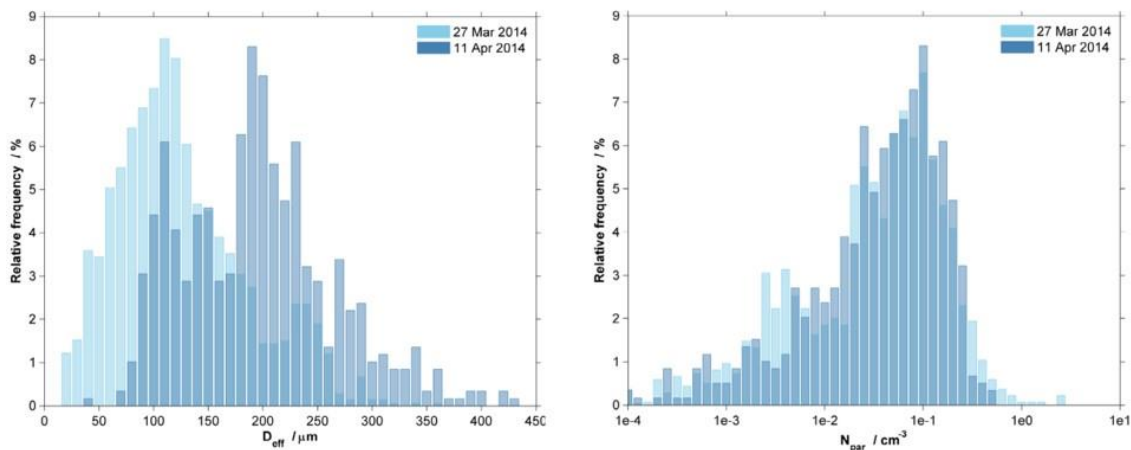
265   **Figure 4: Relative frequency of the derived effective diameter (left) and ice number concentration (right) for the warm conveyor belt cases on 27 March (light blue) and 11 April (dark blue) 2014.**

3.3. In-situ data of all flight missions

Looking at the overall distribution of the derived effective diameter and ice particle number concentration for all cirrus clouds with coordinated lidar and in-situ measurements during ML-CIRRUS (Table 1), we do not find a clear dependence of size and

270   number of ice particles on the PLDR. The median value of D_{eff} (88.6 µm) for the clouds with lower particle linear depolarization ratio is even slightly higher compared to a median D_{eff} of 78.0 µm for the high depolarization mode clouds. The corresponding median values of the ice particle number concentration within this temperature range are quite similar with about 0.05 cm^{-3} for the high and low mode depolarization cirrus. However, for this analysis the whole temperature range from

206 to 238 K is considered. But similar to its impact on the PLDR (Urbanek et al., 2018) the temperature is also correlated
with the mean/median D_{eff} and N_{par} showing lower values for D_{eff} and higher values for N_{par} at the coldest temperature. Looking
at Table 1, one can see that coordinated in-situ and lidar measurements were mainly performed in cirrus clouds formed in
rather from aviation unaffected airmasses and only within a temperature range of 208 K and 217 K. Thus, we use only this
temperature range for a first comparison of D_{eff} and N_{par} for the two cloud classes (Figure 5; left). The median values of D_{eff}
and N_{par} are quite similar for the two cloud classes with slightly larger median D_{eff} value and slightly smaller median N_{par} value
for the high PLDR mode cirrus clouds. But, for the temperature range colder than 209 K in-situ measurements of the high
depolarization mode cirrus clouds are dominating the available data. In contrast, in the temperature range warmer than 215 K
in-situ measurements in cirrus clouds in the low depolarization mode are dominating the data availability. Furthermore, the
available number of data points for temperatures colder than 210 K and warmer than 215 K is small. This might affect the
overall results, as now significant comparison is possible due to the small number of datapoints. Thus, we compare the derived
D_{eff} and N_{par} in a temperature range between 210 K and 215 K (Figure 5; right), where in-situ measurements of both cirrus
cloud types are about available in equal amount. Looking at this temperature regime (210-215 K) one can see slight differences
between the two cirrus cloud classes. Although the main values of D_{eff} for both cloud types are between about 25 µm and
100 µm, the median value of the D_{eff} distribution (50.7 µm) within low mode PLDR cirrus clouds is slightly smaller than the
median D_{eff} value for the in-situ measurements within high mode PLDR cirrus clouds (61.4 µm). The corresponding
distributions of N_{par} show median values of about 0.05 for the high mode PLDR clouds and of 0.11 for the low mode PLDR
clouds.
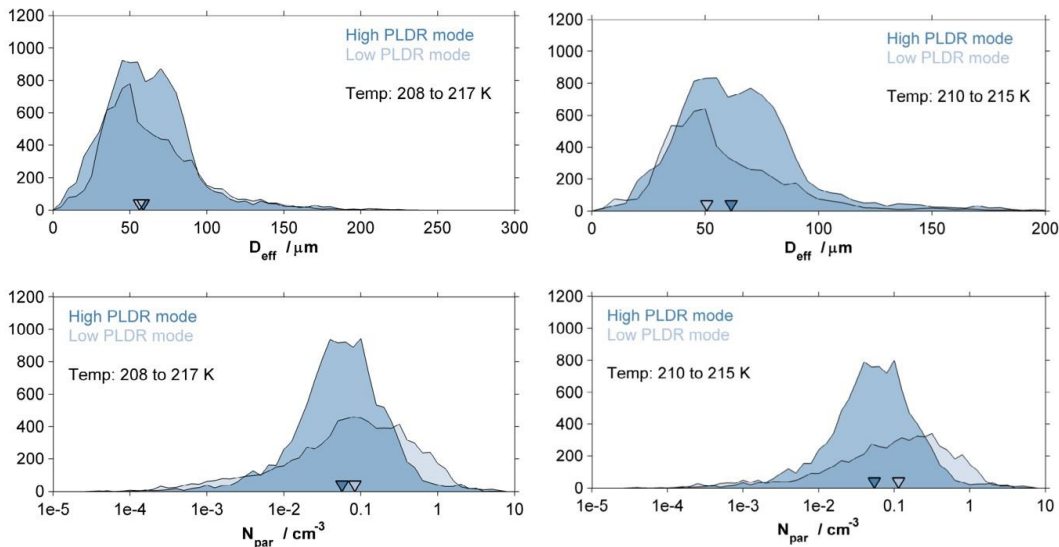
**Figure 5: Probability density function of the measured ice particle effective diameter (upper plots) and ice number concentration
(lower plots) derived from CAS-DLR/CIP-UniM and NIXE-CAPS data (where available) for all cirrus clouds during ML-CIRRUS,
where coordinated lidar and in-situ measurements were available (Table 1) for both cirrus cloud types (PLDR high mode and PLDR**

low mode) (left side) and for those temperature ranges with a significant amount of in-situ samples. The light blue color indicates measurements in low PLDR mode clouds and the one in dark blue show measurements for high PLDR mode clouds.

In a next step, we analyze the temperature dependence of the measured effective diameter and ice particle number concentration. For this evaluation, we use the temperature range from 208 to 217 K, as only in this temperature range we do have data for both cloud types. We derive the distributions of D_{eff} and N_{par} in 1 K steps (Figure 6). As already seen for the overall distribution, we do not find clear differences of D_{eff} for the high mode PLDR clouds and the low mode PLDR clouds for most temperature steps. But again, the distributions are dominated by high mode PLDR clouds in the colder regions and by low mode PLDR clouds in the warmer regions. And, one can see a tendency towards larger D_{eff} with warmer temperatures; which is already known from former studies (e.g. Heymsfield et al., 2010b; Bailey and Hallett, 2009). For the high mode PLDR clouds the median D_{eff} is 22.9 µm at a temperature of 208 K and of 65.4 µm for a temperature of 216 K. The corresponding values for the low mode PLDR clouds are 28.8 µm and 67.2 µm, respectively.
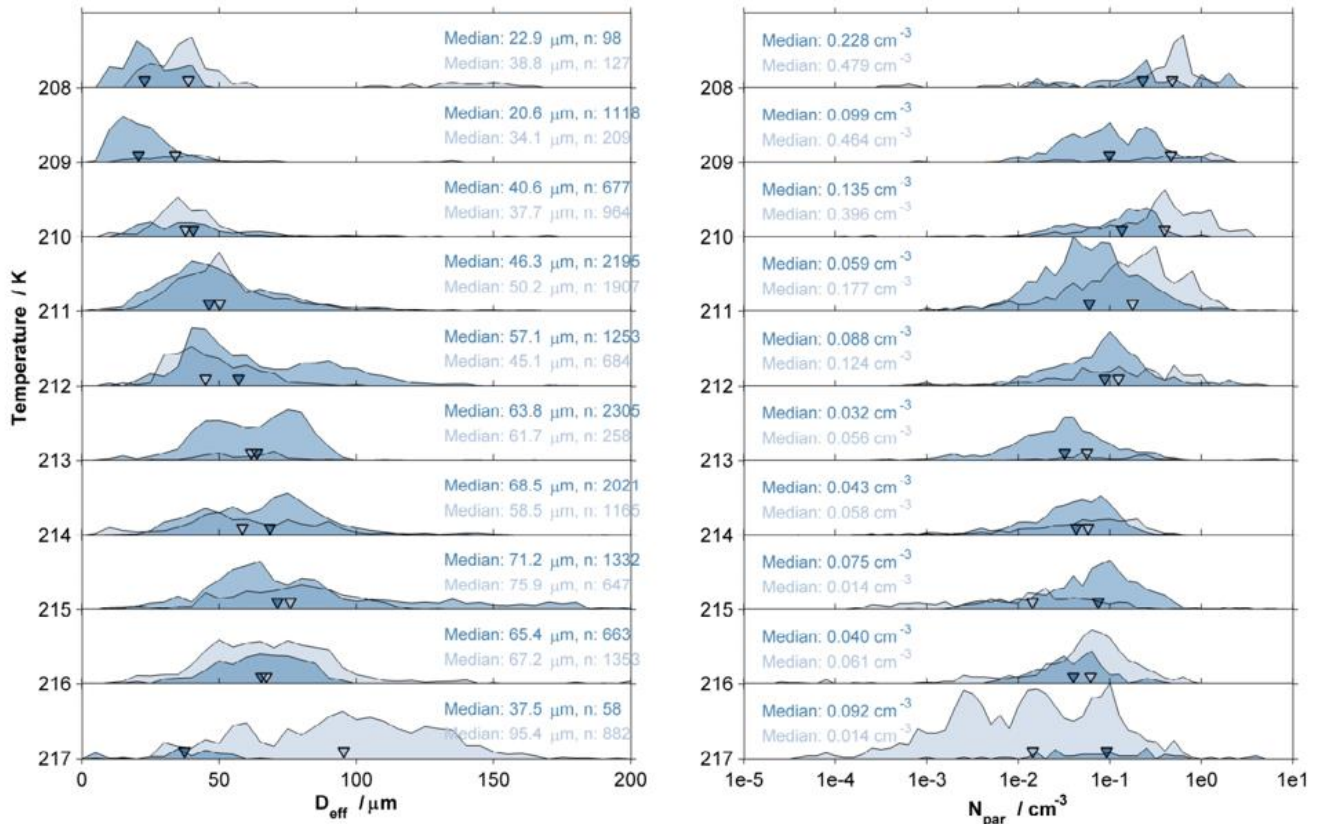
Figure 6: Temperature dependent relative distribution of the measured ice particle effective diameter (left) and ice number concentration (right) derived from CAS-DLR/CIP-UniM and NIXE-CAPS for all cirrus clouds during ML-CIRRUS, where coordinated lidar and in-situ measurements were available (Table 1). The light blue color indicates measurements in low PLDR

mode clouds; the one in dark blue show measurements for high PLDR mode clouds. The triangles indicate the median values and n gives the number of the available datapoints for each comparison.

315   The corresponding distributions of the ice particle number concentration show, that N_{par} is larger for the low mode PLDR cirrus clouds than for the high mode cirrus clouds through all considered temperature ranges with median values of 0.47 cm^{-1} for the low mode PLDR cloud and 0.18 cm^{-1} for the high mode PLDR cloud at a temperature of 208 K, and of about 0.01 cm^{-1} for the low mode PLDR cirrus and about 0.07 cm^{-1} for the high mode PLDR cirrus at a temperature of 215 K. However, as can be seen from Table 1, these last results have to be treated with care, as we have a larger number of high mode cirrus cloud

320   cases in the lower temperature ranges and a dominance of low mode cirrus cloud cases in the higher temperature ranges. Looking only at those temperatures with approximately the same contribution from both cloud types (210-215 K), the distribution of D_{eff} and N_{par} mainly show slightly smaller median particle diameters for the low mode PLDR clouds with corresponding higher median values of the ice particle number concentration.

Discussion and Conclusion

325   In our study, we used the same method and measurements as Urbanek et al (2018), who showed for the first time a difference in the optical properties (i.e. the particle linear depolarization ratio) for cirrus clouds that formed in regions with large aviation induced emissions (having higher values of the PLDR) and those that formed in less affected regions (lower values of the PLDR). We connected the lidar measurements with collocated in-situ measurements of ice particle size and ice particle number concentration from cloud combination probes on HALO, where available.

330   We found, that for those temperature regimes, where we have a sufficient contribution of both cloud types, high PLDR mode clouds show lower ice particle number concentrations with larger effective diameters compared to low PLDR mode clouds. That is an indication for more heterogeneous freezing due to aviation induced emissions, as homogeneous nucleation is expected to be suppressed by heterogeneous nucleation (DeMott et al., 1997; Gierens, 2003). Homogeneous freezing might still occur sometime after the heterogeneous process according to Spichtinger and Cziczo (2010). They further showed, that

335   heterogeneous freezing takes place at lower RHi. In their study, Urbanek et al., (2018) investigated the distribution of RHi inside high mode PLDR clouds and low mode PLDR clouds and found differences in the supersaturation with larger values for the low mode PLDR clouds. These higher values can be thus interpreted such that homogeneous freezing plays a larger role in the low mode PLDR clouds. Homogeneous freezing is expected to produce high ice crystal number concentration and small crystal sizes (Kärcher et la., 2006, Spichtinger and Cziczo, 2010; Krämer et al., 2016). This was found during the

340   COVID-19 curfew with strongly reduced aviation (Zhu et al., 2022) and thus decreased number of ice nucleating particles (INP). In the presence of solid aerosol particles that act as INP, ice crystals form at lower supersaturation. The INP are comparably less numerous than the small aerosol solution droplets causing homogeneous freezing. Thus, the available water vapor deposits on a smaller number of ice crystals but grow to larger sizes and potentially also more complex ice crystals

(Schnaiter et la., 2016). The availability of INP and thus heterogeneous freezing processes lead furthermore to lower number ice particle number concentration in a subsequent homogeneous freezing process compared to pure homogenous freezing (Spichtinger and Cziczo, 2010; Krämer et al., 2016). This effect is stronger the more INP are available.

The differences of D_{eff} and N_{par} for the high and low mode PLDR clouds, with larger N_{par} but slightly smaller D_{eff} for the low mode PLDR clouds, can thus also be interpreted as traces of more frequent heterogeneous freezing in the high mode PLDR clouds. Similar results were also found in a recent study investigating the changes in ice crystal number concentration during the COVID-19 caused air traffic closure (Zhu et al., 2022). They found a reduction in the ice crystal number concentration during that period and interpreted it as an increase in homogeneous freezing as soot from aircraft emissions was reduced. Li and Groß (2021) investigated the optical properties of cirrus clouds over the European Mid-Latitudes and found a reduction in the PLDR of cirrus clouds during the COVID-19 lockdown in spring 2020. However, number concentration and crystal size are not expected to be the only microphysical properties to affect the measured particle linear depolarization ratio, directly. It also depends on the crystal habit or surface roughness, thus on the complexity of the particles. Conditions during the nucleation process (e.g. temperature, relative humidity) impact the ice crystal shape (Bailey and Hallett, 2009). More heterogeneous freezing at lower supersaturation (Urbanek et al., 2018) and warmer temperature regimes (Kanitz et al., 2011) as expected for the high mode PLDR might lead to changes in the ice crystal complexity. Larger particles with more complex structure where found e.g. from balloon-borne measurements of cirrus clouds (Heymsflield, 2003) under such conditions. In this study, we also find a temperature dependence of D_{eff} and N_{par} with larger D_{eff} and lower N_{par} for the warmer cloud temperature range. Although the ML-CIRRUS campaign was not designed to investigate an indirect aviation effect of cirrus clouds and aerosols in the regions of cirrus cloud formation were not explored in detail, it was possible to derive important information of the data. Furthermore, the original focus of ML-CIRRUS was not on a sufficient collocation of lidar and in-situ measurements for both cloud types. Therefore, additional measurements were performed during the CIRRUS-HL mission in 2021 and the flight planning for the CIRRUS-HL campaign learned from our experiences and the collocation of lidar and in-situ measurements was particularly improved. Also, the sampling of aerosol properties in the region of the cloud formation and evolution was a focus of CIRRUS-HL. In the following, we expect that data from the CIRRUS-HL mission will address more of the open questions related to the impact of aviation on ice cloud properties, e.g. how the PLDR and microphysical properties depend on the aerosol concentration and size distribution in the region of cloud evolution.

Data availability

The data used in this study are available at the HALO database (halo-db.pa.op.dlr.de).

Author contributions

375 SG performed the lidar measurements, CV, TJW, MK performed the in-situ measurements during ML-CIRRUS. MW provided the basic analysis of the lidar data. MK, TJW provided the basic analysis of the in-situ data. BU, QL, SG preformed the analyzes in this study. SG wrote the manuscript. All authors discussed the data and findings.

Acknowledgements

ML-CIRRUS was mainly funded by the Deutsches Zentrum für Luft- und Raumfahrt (DLR), and the Deutsche Forschungsgesellschaft (DFG) within the SPP1294-HALO under contract VO1504/7-1, and by the Helmholtz Association 380 under contract W2/W3-60. This study was funded by CRC project TRR 301 under Project-ID 428312742, and DLR internal funding within the MABAK project.

References

Bailey, M. P. and Hallett, J.: A comprehensive habit diagram for atmospheric ice crystals: Confirmation from the laboratory, AIRS II, and other field studies, J. Atmos. Sci., 66, 2888–2899, 2009.

385 Bock, L. and Burkhardt, U.: Contrail cirrus radiative forcing for future air traffic, Atmos. Chem. Phys., 19, 8163–8174, https://doi.org/10.5194/acp-19-8163-2019, 2019.

Bräuer, T., Voigt, C., Sauer, D., Kaufmann, S., Hahn, V., Scheibe, M., Schlager, H., Huber, F., Le Clercq, P., Moore, R. H., and Anderson, B. E.: Reduced ice number concentrations in contrails from low-aromatic biofuel blends, Atmos. Chem. Phys., 21, 16817–16826, https://doi.org/10.5194/acp-21-16817, 2021.

390 Browning, K. A.: Radar measurements of air motion near fronts. Weather, 26(8), 320-340, 1971.

Burkhardt, U. and Kärcher, B.: Global radiative forcing from contrail cirrus, Nature Climate Change, 1 (1), 54–58, doi:10.1038/nclimate1068, 2011.

Burkhardt, U., Kärcher, B., and Schumann U.: Global modeling of the contrail and contrail cirrus climate impact, Bulletin of the American Meteorological Society, 91 (4), 479–484, doi:10.1175/2009bams2656.1, 2010.

395 Costa, A., Meyer, J., Afchine, A., Luebke, A., Günther, G., Dorsey, J. R., Gallagher, M. W., Ehrlich, A., Wendisch, M., Baumgardner, D., Wex, H., and Krämer, M.: Classification of Arctic, midlatitude and tropical clouds in the mixed-phase temperature regime, Atmos. Chem. Phys., 17, 12219–12238, https://doi.org/10.5194/acp-17-12219-2017, 2017.

DeMott, P., D. Cziczo, D., Prenni, A., Murphy, D., Kreidenweis, S., Thomson, D., Borys, R., and Rogers, D.: Measurements of the concentration and composition of nuclei for cirrus formation, Proc. Natl. Acad. Sci. U. S. A., 100, 14,655–14,660,

400 2003.

DeMott, P. Sassen, J., K., Poellot, M. R., Baumgardner, D., Rogers, D.C., Brooks, S. D., Prenni, A. J., and Kreidenweis, S. M.: African dust aerosols as atmospheric ice nuclei. Geophys. Res. Lett., **30**, 1732, doi:10.1029/2003GL017410, 2003.

Eckhardt, S., Stohl, A., Wernli, H., James, P., Forster, C., and Spichtinger, N.: A 15-year climatology of warm conveyor belts. Journal of climate, 17(1), 218-237, 2004.

405 Esselborn, M., Wirth, M., Fix, A., Tesche, M., and Ehret, G.: Airborne high spectral resolution lidar for measuring aerosol extinction and backscatter coefficients, Applied Optics, 47 (3), 346, doi:10.1364/ao.47.000346, 2008.

Freudenthaler, V., Esselborn, M., Wiegner, M., Heese, B., Tesche, M., Ansmann, A., Müller, D., Althausen, D., Wirth, M., Fix, A., Ehret, G., Knippertz, P., Toledano, C., Gasteiger, J., Garhammer, M., and Seefeldner, M.: Depolarization ratio profiling at several wavelengths in pure saharan dust during SAMUM 2006, Tellus B: Chemical and Physical Meteorology, 61 (1), 165–
410 179, doi:10.1111/j.1600-0889.2008.00396.x, 2009.

Gettelman, A. and Chen, C.: The climate impact of aviation aerosols, Geophys. Res. Lett., 40, 2785–2789, https://doi.org/10.1002/grl.50520, 2013.

Gierens, K. M.: On the transition between heterogeneous and homogeneous freezing, Atmos. Chem. Phys., 3, 437–446, 2003.

Hendricks, J., Kärcher, B., Lohmann, U., and Ponater, M.: Do aircraft black carbon emissions affect cirrus clouds on the global
415 scale?, Geophys. Res. Lett., 32, 12, https://doi.org/10.1029/2005gl022740, 2005.

Giez, A., Zöger, M., Mallaun, C., Nenakhov, V., Schimpf, M., Grad, C., Numberger, A. and Raynor, K.: Determination of the measurement errors for the HSLO basic data System BAHAMAS by means of error propagation, DLR-FB 2022-27. 97, doi:10.57676/5rdc-q708, 2023.

Grewe, V., Dahlmann, K., Flink, J., Frömming, C., Ghosh, R., Gierens, K., Heller, R., Hendricks, J., Jöckel, P., Kaufmann, S.,
420 Kölker, K., Linke, F., Luchkova, T., Lührs, B., van Manen, J., Matthes, S., Minikin, A., Niklaß, M., Plohr, M., Righi, M., Rosanka, S., Schmitt, A., Schumann, U., Terekhov, I., Unterstrasser, S., Vázquez-Navarro, M., Voigt, C., Wicke, K., Yamashita, H., Zahn, A., Ziereis, H., Mitigating the Climate Impact from Aviation: Achievements and Results of the DLR WeCare Project Aerospace, 4(3), 34; doi:10.3390/aerospace4030034, 2017.

Groß, S., M. Wirth, A. Schäfler, A. Fix, S. Kaufmann, and C. Voigt: Potential of airborne lidar measurements for cirrus cloud
425 studies, Atmos. Meas. Tech., 7, 2745-2755, doi:10.5194/amt-7-2745-2014, 2014.

Hendricks, J., Kärcher, B., and Lohmann, U.: Effects of ice nuclei on cirrus clouds in a global climate model, J. Geophys. Res.-Atmos., 116, D18, https://doi.org/10.1029/2010jd015302, 2011.

Heymsfield, A. J.: Properties of tropical and midlatitude ice cloud particle ensembles. Part I: Median mass diameters and terminal velocities, J. Atmos. Sci., 60, 2573–2591, 2003.

430 Heymsfield, A., Baumgardner, D., DeMott, P., Forster, P., Gierens, K., and Kärcher, B.: Contrail microphysics, Bulletin of the American Meteorological Society, 91 (4), 465–472, doi:10.1175/2009bams2839.1, 2010a.

Heymsfield, A. J., Schmitt, C., Bansemer, A., and Twohy, C. H.: Improved representation of ice particle masses based on observations in natural clouds. Journal of the Atmospheric Sciences, 67(10), 3303-3318, 2010b.

Haywood, J. M., Allan, R. P., Bornemann, J., Forster, P. M., Francis, P. N., Milton, S., Rädel, G., Rap, A., Shine, K. P., and
435 Thorpe, R.: A case study of the radiative forcing of persistent contrails evolving into contrail-induced cirrus, J. Geophys. Res., 114, D24201, doi:10.1029/2009JD01265, 2009.

Hoose, C. and Möhler, O.: Heterogeneous ice nucleation on atmospheric aerosols: a review of results from laboratory experiments, Atmos. Chem. Phys., 12, 9817–9854, https://doi.org/10.5194/acp-12-9817-2012, 2012.

Kärcher, B., Burkhardt, U., Bier, A., Bock, L., and Ford, I. J.: The microphysical pathway to contrail formation, Journal of

440   Geophysical Research: Atmospheres, 120 (15), 7893–7927, doi:10.1002/2015jd023491, 2015.

Kärcher, B.: Cirrus Clouds and Their Response to Anthropogenic Activities, Curr. Clim. Change Rep., 3, 45–57, https://doi.org/10.1007/s40641-017-0060-3, 2017.

Kärcher, B.: Formation and radiative forcing of contrail cirrus, Nature Communications, 9 (1), doi:10.1038/s41467-018-04068-0, 2018.

445   Kanitz, T., Seifert, P., Ansmann, A., Engelmann, R., Althausen, D., Casiccia, C., and Rohwer, E. G.: Contrasting the impact of aerosols at northern and southern midlatitudes on heterogeneous ice formation. Geophysical Research Letters, 38(17), 2011.

Kaufmann, S., Voigt, C., Heller, R., Jurkat-Witschas, T., Krämer, M., Rolf, C., Zöger, M., Giez, A., Buchholz, B., Ebert, V., Thornberry, T., and Schumann, U.: Intercomparison of midlatitude tropospheric and lower-stratospheric water vapor measurements and comparison to ECMWF humidity data, Atmos. Chem. Phys., 18, 16729–16745,

450   https://doi.org/10.5194/acp-18-16729-2018, 2018.

Krämer, M., Rolf, C., Luebke, A., Afchine, A., Spelten, N., Costa, A., Meyer, J., Zöger, M., Smith, J., Herman, R. L., Buchholz, B., Ebert, V., Baumgardner, D., Borrmann, S., Klingebiel, M., and Avallone, L.: A microphysics guide to cirrus clouds – Part 1: Cirrus types, Atmos. Chem. Phys., 16, 3463–3483, https://doi.org/10.5194/acp-16-3463-2016, 2016.

Li, Q. and Groß, S.: Changes in cirrus cloud properties and occurrence over Europe during the COVID-19-caused air traffic

455   reduction, Atmos. Chem. Phys., 21, 14573–14590, https://doi.org/10.5194/acp-21-14573-2021, 2021.

Li, Q. and Groß, S.: Satellite observations of seasonality and long-term trend in cirrus cloud properties over Europe: Investigation of possible aviation impacts, submitted to ACP

Liu, X., Penner, J. E., and Wang, M.: Influence of anthropogenic sulfate and black carbon on upper tropospheric clouds in the NCAR CAM3 model coupled to the IMPACT global aerosol model, J. Geophys. Res.-Atmos., 114,

460   D3, https://doi.org/10.1029/2008jd010492, 2009.

Lund, M. T., Aamaas, B., Berntsen, T., Bock, L., Burkhardt, U., Fuglestvedt, J. S., and Shine, K. P.: Emission metrics for quantifying regional climate impacts of aviation, Earth System Dynamics, 8 (3), 547–563, doi:10.5194/esd-8-547-2017, 2017.

Mahrt, F., Kilchhofer, K., Marcolli, C., Grönquist, P., David, R. O., Rösch, M., Lohmann, U., and Kanji, Z. A.: The Impact of Cloud Processing on the Ice Nucleation Abilities of Soot Particles at Cirrus Temperatures, J. Geophys. Res.-Atmos., 125,

465   3, https://doi.org/10.1029/2019jd030922, 2020.

Marjani, S., Tesche, M., Bräuer, P., Sourdeval, O., and Quaas, J.: Satellite observations of the impact of individual aircraft on ice crystal number in thin cirrus clouds, Geophysical Research Letters, 49, https://doi.org/10.1029/2021GL096173, 2022.

McKenna, D. S.: A new Chemical Lagrangian Model of the Stratosphere (CLaMS) 1. formulation of advection and mixing, Journal of Geophysical Research, 107 (D16), doi:10.1029/2000jd000114. 2002.

470   Möhler, O., Büttner, S., Linke, C., Schnaiter, M., Saathoff, H., Stetzer, O., Wagner, R., Krämer, M., Mangold, A., Ebert, V., and Schurath, U.: Effect of sulfuric acid coating on heterogeneous ice nucleation by soot aerosol particles, J. Geophys. Res.-Atmos., 110, D11, https://doi.org/10.1029/2004jd005169, 2005.

Moore, R. H., Thornhill, K. L., Weinzierl, B., Sauer, D., D'Ascoli, E., Kim, J., Lichtenstern, M., Scheibe, M., Beaton, B., Beyersdorf, A. J., Barrick, J., Bulzan, D., Corr, C. A., Crosbie, E., Jurkat, T., Martin, R., Riddick, D., Shook, M., Slover, G.,

475   Voigt, C., White, R., Winstead, E., Yasky, R., Ziemba, L. D., Brown, A., Schlager, H., and Anderson, B. E.: Biofuel blending reduces particle emissions from aircraft engines at cruise conditions, Nature, 543, 411-415, 10.1038/nature21420, 2017.

Penner, J. E., Chen, Y., Wang, M., and Liu, X.: Possible influence of anthropogenic aerosols on cirrus clouds and anthropogenic forcing, Atmos. Chem. Phys., 9, 879–896, https://doi.org/10.5194/acp-9-879-2009, 2009.

Penner, J. E., Zhou, C., Garnier, A., and Mitchell, D. L.: Anthropogenic Aerosol Indirect Effects in Cirrus Clouds, J. Geophys.

480   Res.-Atmos., 123, 11652–11677, https://doi.org/10.1029/2018jd029204, 2018.

Quaas, J., Gryspeerdt, E., Vautard, R., and Boucher, O.: Climate impact of aircraft-induced cirrus assessed from satellite observations before and during COVID-19, Environ. Res. Lett., 16, 064051, https://doi.org/10.1088/1748-9326/abf686, 2021.

Righi, M., Hendricks, J., Lohmann, U., Beer, C. G., Hahn, V., Heinold, B., Heller, R., Krämer, M., Ponater, M., Rolf, C., Tegen, I., and Voigt, C.: Coupling aerosols to (cirrus) clouds in the global EMAC-MADE3 aerosol–climate model, Geosci.

485   Model Dev., 13, 1635–1661, https://doi.org/10.5194/gmd-13-1635-2020, 2020

Righi, M., Hendricks, J., and Beer, C. G.: Exploring the uncertainties in the aviation soot–cirrus effect, Atmospheric Chemistry and Physics, (17267-17289), 10.5194/acp-21-17267-2021, 21, 23, 2021.

Schumann, U.; Mayer, B.; Gierens, K.; Unterstrasser, S.; Jessberger, P.; Petzold, A.; Voigt, C. & Gayet, J.-F.

Effective Radius of Ice Particles in Cirrus and Contrails, Journal of the Atmospheric Sciences, American Meteorological

490   Society, 2011, 68, 300 - 321

Schumann, U.: A contrail cirrus prediction model, Geosci. Model Dev., 5, 543–580, https://doi.org/10.5194/gmd-5-543-2012, 2012.

Schnaiter, M., Järvinen, E., Vochezer, P., Abdelmonem, A., Wagner, R., Jourdan, O., Mioche, G., Shcherbakov, V. N., Schmitt, C. G., Tricoli, U., Ulanowski, Z., and Heymsfield, A. J.: Cloud chamber experiments on the origin of ice crystal

495   complexity in cirrus clouds, Atmos. Chem. Phys., 16, 5091–5110, https://doi.org/10.5194/acp-16-5091-2016, 2016.

Schumann, U., Baumann, R., Baumgardner, D., Bedka, S. T., Duda, D. P., Freudenthaler, V., Gayet, J.-F., Heymsfield, A. J., Minnis, P., Quante, M., Raschke, E., Schlager, H., Vazquez-Navarro, M., Voigt, C., and Wang, Z.: Properties of individual contrails: a compilation of observations and some comparisons, Atmospheric Chemistry and Physics, 17 (1), 403–438, doi:10.5194/acp-17-403-2017, 2017.

500   Schumann, U., Poll, I., Teoh, R., Koelle, R., Spinielli, E., Molloy, J., Koudis, G. S., Baumann, R., Bugliaro, L., Stettler, M., and Voigt, C.: Air traffic and contrail changes over Europe during COVID-19: a model study, Atmos. Chem. Phys., 21, 7429–7450, https://doi.org/10.5194/acp-21-7429-2021, 2021a.

Schumann, U., Bugliaro, L., Dörnbrack, A., Baumann, R., and Voigt, C.: Aviation contrail cirrus and radiative forcing over Europe during 6 months of COVID-19, Geophys. Res. Lett., 48, e2021GL092771, https://doi.org/10.1029/2021GL092771, 2021b.

Spichtinger, P. and Cziczo, D. J.: Impact of heterogeneous ice nuclei on homogeneous freezing events in cirrus clouds, Journal of Geophys. Res., 115, D14, https://doi.org/10.1029/2009JD012168, 2010

Teoh, R., Schumann, U., Gryspeerdt, E., Shapir, M., Molloy, J., Koudis, G., Voigt, C., and Stettler, E., J.: Aviation contrail climate effects in the North Atlantic from 2016 to 2021. Atmos. Chem. Phys., 22, 10919-10935, https://doi.org/10.5194/acp-22-10919-2022, 2022.

Tesche, M., Achtert, P., Glantz, P., and Noone, K. J.: Aviation effects on already-existing cirrus clouds, Nat. Commun., 7, 12016, https://doi.org/10.1038/ncomms12016, 2016.

Urbanek, B.: Characterization of midlatitude cirrus clouds with airborne lidar - Investigating an indirect aviation effect. Diss. LMU, 2019.

Urbanek, B., Groß, S., Schäfler, A., and Wirth, M.: Determining stages of cirrus evolution: a cloud classification scheme, Atmos. Meas. Tech., 10, 1653–1664, https://doi.org/10.5194/amt-10-1653-2017, 2017.

Urbanek, B., Groß, S., Wirth, M., Rolf, C., Krämer, M., and Voigt, C.: High depolarization ratios of naturally occurring cirrus clouds near air traffic regions over Europe, Geophys. Res. Lett., 45, 13166–13172, https://doi.org/10.1029/2018GL079345, 2018.

Voigt, C., U. Schumann, T. Jurkat, D. Schäuble, H. Schlager, A. Petzold, J.-F. Gayet, M. Krämer, J. Schneider, S. Borrmann, J. Schmale, P. Jessberger, T. Hamburger, M. Lichtenstern, M. Scheibe, C. Gourbeyre, J. Meyer, M. Kübbeler, W. Frey, H. Kalesse, T. Butler, M. G. Lawrence, F. Holzäpfel, F. Arnold, M. Wendisch, A. Döpelheuer, K. Gottschaldt, R. Baumann, M. Zöger, I. Sölch, M. Rautenhaus, and A. Dörnbrack: In-situ observations of young contrails - Overview and selected case studies from the CONCERT campaign, Atmos. Chem. Phys., 10, 9039–9056, www.atmos-chem-phys.net/10/9039/2010, doi:10.5194/acp-10-9039-2010, 2010.

Voigt, C., Schumann, U., Minikin, A., Abdelmonem, A., Afchine, A., Borrmann, S., Boettcher, M., Buchholz, B., Bugliaro, L., Costa, A., Curtius, J., Dollner, M., Dörnbrack, A., Dreiling, V., Ebert, V., Ehrlich, A., Fix, A., Forster, L., Frank, F., Fütterer, D., Giez, A., Graf, K., Grooß, J.-U., Groß, S., Heimerl, K., Heinold, B., Hüneke, T., Järvinen, E., Jurkat, T., Kaufmann, S., Kenntner, M., Klingebiel, M., Klimach, T., Kohl, R., Krämer, M., Krisna, T. C., Luebke, A., Mayer, B., Mertes, S., Molleker, S., Petzold, A., Pfeilsticker, K., Port, M., Rapp, M., Reutter, P., Rolf, C., Rose, D., Sauer, D., Schäfler, A., Schlage, R., Schnaiter, M., Schneider, J., Spelten, N., Spichtinger, P., Stock, P., Walser, A., Weigel, R., Weinzierl, B., Wendisch, M., Werner, F., Wernli, H., Wirth, M., Zahn, A., Ziereis, H., and Zöger, M.: ML-CIRRUS: The airborne experiment on natural cirrus and contrail cirrus with the high-altitude long-range research aircraft HALO, B. Am. Meteorol. Soc., 98, 271–288, https://doi.org/10.1175/BAMS-D-15-00213.1, 2017.

Voigt, C., Lelieveld, J., Schlager, H., Schneider, J., Curtius, J., Meerkötter, R., Sauer, D., Bugliaro, L., Bohn, B., Crowley, J. N., Erbertseder, T., Groß, S., Hahn, V., Li, Q., Mertens, M., Pöhlker, M. L., Pozzer, A., Schumann, U., Tomsche, L., Williams,

J., Zahn, A., Andreae, M., Borrmann, S., Bräuer, T., Dörich, R., Dörnbrack, A., Edtbauer, A., Ernle, L., Fischer, H., Giez, A., Granzin, M., Grewe, V., Harder, H., Heinritzi, M., Holanda, B. A., Jöckel, P., Kaiser, K., Krüger, O. O., Lucke, J., Marsing, A., Martin, A., Matthes, S., Pöhlker, C., Pöschl, U., Reifenberg, S., Ringsdorf, A., Scheibe, M., Tadic, I., Zauner-Wieczorek,

540   M., Henke, R., and Rapp, M.: Cleaner skies during the COVID-19 lockdown, Bulletin of the American Meteorological Society, doi.org/10.1175/BAMS-D-21-0012.1, 2022.

Wang, Z., Bugliaro, L., Jurkat-Witschas, T., Heller, R., Burkhardt, U., Ziereis, H., Dekoutsidis, G., Wirth, M., Groß, S., Kirschler, S., Kaufmann, S., and Voigt, C.: Observations of microphysical properties and radiative effects of a contrail cirrus outbreak over the North Atlantic, Atmos. Chem. Phys., 23, 1941–1961, https://doi.org/10.5194/acp-23-1941-2023, 2023.

545   Weigel, R., Spichtinger, P., Mahnke, C., Klingebiel, M., Afchine, A., Petzold, A., Krämer, M., Costa, A., Molleker, S., Reutter, P., Szakáll, M., Port, M., Grulich, L., Jurkat, T., Minikin, A., and Borrmann, S.: Thermodynamic correction of particle concentrations measured by underwing probes on fast-flying aircraft, Atmos. Meas. Tech., 9, 5135–5162, https://doi.org/10.5194/amt-9-5135-2016, 2016.

Winker, D. M., Pelon, J., Coakley Jr., J. A., Ackerman, S. A., Charlson, R. J., Colarco, P. R., Flamant, P., Fu, Q., Hoff, R. M.,

550   Kittaka, C., Kubar, T. L., Le Treut, H., Mccormick, M. P., Mégie, G., Poole, L., Powell, K., Trepte, C., Vaughan, M. A., and Wielicki, B. A.: The CALIPSO Mission: A global 3D view of aerosols and clouds, B. Am. Meteorol. Soc., 91, 1211–1229, https://doi.org/10.1175/2010BAMS3009.1, 2010.

Wirth, M., Fix, A., Mahnke, P., Schwarzer, H., Schrandt, F., and Ehret, G.: The airborne multi-wavelength water vapor differential absorption lidar WALES: system design and performance, Applied Physics B, 96 (1), 201–213,

555   doi:10.1007/s00340-009-3365-7, 2009.

Zhou, C. and Penner, J. E.: Aircraft soot indirect effect on large-scale cirrus clouds: Is the indirect forcing by aircraft soot positive or negative?, J. Geophys. Res.-Atmos., 119, 11303–11320, https://doi.org/10.1002/2014jd021914, 2014.

Zhu, J., Penner, J. E., Garnier, A., Boucher, O., Gao, M., Song, L., Deng, J., Liu, C, and Fu, P.: Decreased aviation leads to increased ice crystal number and a positive radiative effect in cirrus clouds. AGU Advances, 3(2),

560   https://doi.org/10.1029/2021AV000546, 2022.